Letters on Materials 16 (1), 2026 pp. 71-77 www.lettersonmaterials.com

Received 13 November 2025; Accepted 12 January 2026
https://doi.org/10.48612/letters/2026-1-71-77 https://elibrary.ru/votfea

Estimation of elastic modulus anisotropy in grain-oriented electrical steel using EBSD and DMA methods

S. I. Stepanov[1], M. A. Zorina[1], D. D. Satskii[1,3], M. S. Karabanalov[1], M. P. Puzanov[3],

Yu. N. Loginov[1,2], M. L. Lobanov[†1,2]

[†]m.l.lobanov@urfu.ru

[1]Ural Federal University, Ekaterinburg 620002, Russia
[2]M. N. Mikheev Institute of Metal Physics, Ural Branch of the Russian Academy of Sciences, Ekaterinburg 620108, Russia
[3]PJSC Novolipetsk Steel plant (NLMK), Lipetsk 398040, Russia

Abstract: Grain-oriented electrical steel (GOES) is characterized by a strong crystallographic texture, which is crucial for its magnetic properties. However, this texture also induces significant anisotropy in its elastic characteristics, which is less studied but important for manufacturing and application. This work investigates the anisotropy of the elastic modulus in GOES at different stages of its production — specifically after the first cold rolling (CR1), after subsequent decarburization–recrystallization annealing (DRA), and after the second cold rolling (CR2). The study employs a combined approach using Electron Backscatter Diffraction (EBSD) for texture analysis and Dynamic Mechanical Analysis (DMA) for direct measurement of storage modulus. Using the EBSD analysis the evolution of the crystallographic texture across the manufacturing stages was studied. The key texture components were qualified and quantified by 20° deviation of standard crystallographic directions <100>, <110> and <111> from CR axes: RD, TD and ND. These data were compared to the spatial maps of Young's modulus, showing a uniform distribution in the rolling direction (RD) and the greatest dispersion of values in the normal direction (ND) for all processing stages. The maximum modulus values were consistently observed in the transverse direction (TD). A comparative analysis demonstrated a correlation between the elastic moduli values obtained via EBSD calculations and direct DMA measurements. A more significant divergence was noted for the thinner CR2 sheet (0.27 mm), which is attributed to the specific stress state during three-point bending in DMA, which amplifies the contribution of the near-surface layers.

Keywords: transformer steel, electrical steel, soft ferromagnetic material, Goss texture, elastic properties anisotropy, dynamic mechanical analysis, BCC, EBSD, GOES, cold rolling, recrystallization annealing

Acknowledgements: *This work was carried out with the financial support of the Russian Science Foundation (RSF) grant No. 25-19-00683, https://rscf.ru/project/25-19-00683/.*

1. Introduction

Grain oriented electrical steel (GOES) is the basic material used in transformer cores production. A key requirement for GOES is high magnetic properties in rolling direction, achieved through sharp crystallographic texture formation with a {110}<001> component in finished products. Required magnetic properties anisotropy in rolling direction is achieved by the [001] preferential orientation of the grains, which is the easiest magnetization axis in bcc iron [1–3].

The development of the required texture in finished products occurs during high-temperature annealing as a result of secondary recrystallization (SR), which leads to the formation of a coarse-grained structure (grain size in the sheet plane of 5–30 mm) with a perfect crystallographic texture. Key conditions for successful course of SR are the presence of predominant {110}<001> orientation grains and the inhibitor phase, which hinders boundary movement and is capable of gradual coagulation and subsequent dissolution in the SR temperature range [4–7].

Creating favorable conditions for the SR process is the main task of the GOES production technological chain, which includes several stages: smelting, hot rolling, two stages cold rolling separated by recrystallization-decarburization annealing, high-temperature and flattening annealing [8,9]. Each technological operation affects the material's structural and textural states, thus creating and changing the anisotropy of physical and mechanical properties in the strip via deformation and heat treatment [10–14].

Controlling the anisotropy of physical and mechanical properties at various industrial production stages should improve the accuracy of the modeling process and lay the foundation for developing methods for characterizing small-section semi-finished products. Currently, modern methods allow us to evaluate the physical and mechanical properties of the materisl with sufficient accuracy [15–17].

This work is devoted to the investigation of the influence of the grain oriented silicon steel's structural and textural states on the anisotropy of elastic properties using the methods of orientation microscopy and dynamic mechanical analysis.

2. Materials and methods

The work was carried out on commercial GOES sheets, manufactured according to the Russian technology type described in [8]. The first batch of the samples was taken after the first cold rolling (CR1) with a strain of 72% from the sheet with a thickness of 0.7 mm; the second batch of the samples was taken after decarburization-recrystallization annealing (DRA) in a 95%N_2 + 5%H_2 humidified atmosphere (CR1+DRA) and the third batch was taken after the second cold rolling (CR2) with a strain of 63% to a thickness of 0.26 mm.

The electron microscopic examination was performed using a ThermoScientific Scios 2 LoVac scanning electron microscope at an accelerating voltage of 20 kV. An Oxford Instruments Symmetry EBSD Detector was used to determine individual grains orientations and analyze the texture through the sheet thickness. The scanning step was 0.5 μm. The error in determining crystal lattice orientation was ±1° (±0.6° on average). The EBSD data were analyzed using the AZtec Crystal software.

The dynamic mechanical analysis (DMA) was employed on a NETZSCH DMA 242 with three-point bending loading applied to $20 \times 4 \times h$ mm specimens (where h is the sheet thickness) to determine the alloy's storage modulus. A sinusoidal cyclic load of 5.3 N was applied to the specimen at a frequency of 1 Hz.

3. Results and discussion

The texture analysis of a 0.7 mm thick sheet after the CR1 demonstrated a standard set of orientations for BCC metals [18–22]. The main orientation typical with a maximum density of 15.9 for elongated deformed grains is a stable deformation cube {001}<110> (Fig. 1a) along with the noted α-fiber {113}<110> and {112}<110> orientations typical for grains that have undergone significant fragmentation. The misorientation between the fragments reaches angles of more than 20° (Fig. 1a). In addition, low-intensity γ-fiber components are found in ODF section φ2 = 45° (Fig. 2a). The maximum degree of fragmentation and significant structure refinement are observed for these areas. Texture representation in the form of fibers indicates the certain

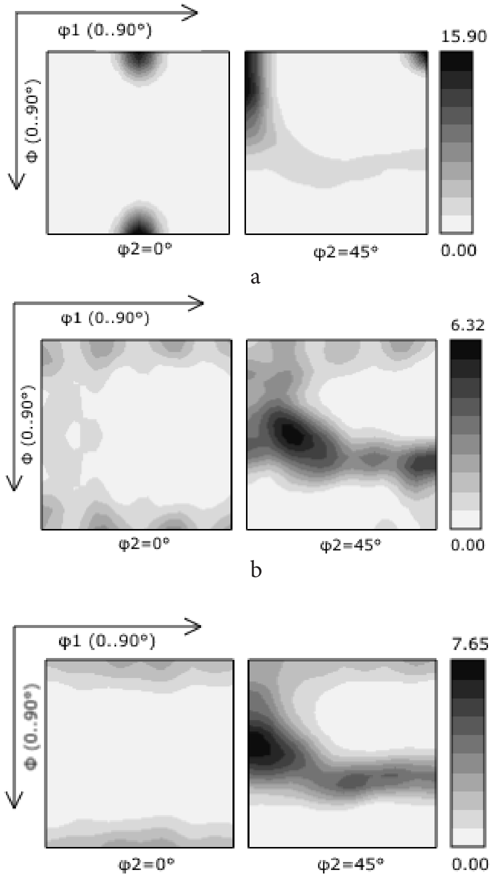

Fig. 2. ODF φ2 = 0 and φ2 = 45° sections for GOES sheets at different processing stages: 0.7 mm after CR1 (a), 0.7 mm after CR1+DRA (b), 0.27 mm after CR2 (c).

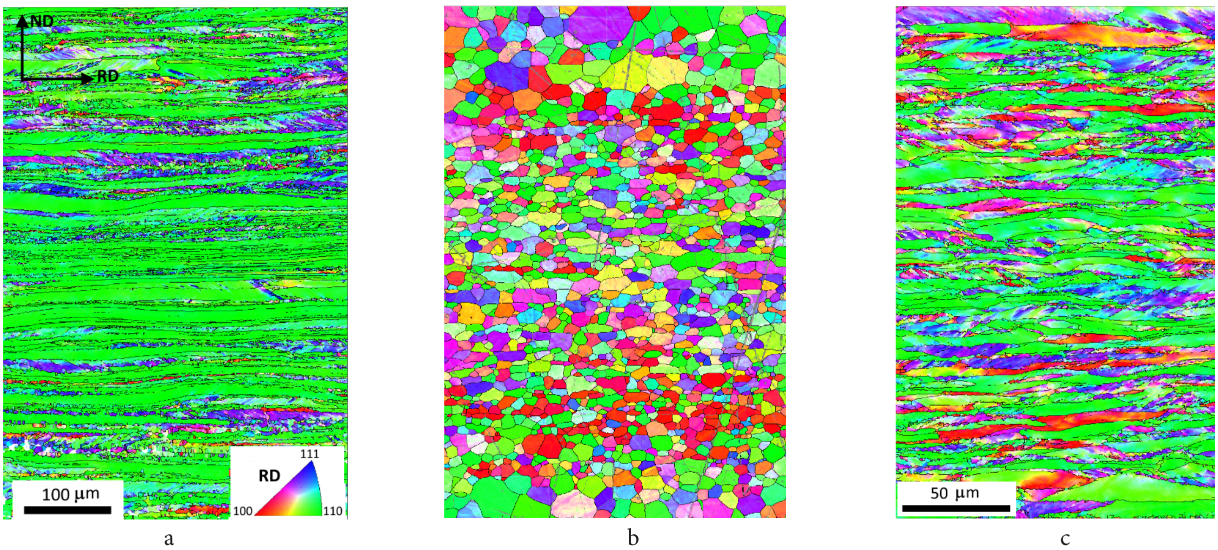

Fig. 1. (Color online) IPF colored maps for full thickness of the GOES sheets at different processing stages: 0.7 mm after CR1 (a); 0.7 mm after CR1+DRA (b), 0.27 mm after CR2 (c).

crystallographic direction predominance relative to the stress state acting during rolling. In particular, α-fiber assumes a preferential orientation of <110> direction along the RD, and γ-fiber assumes a preferential orientation of <111> along ND. In general, the structural and textural state is typical for metals with a BCC lattice after cold rolling [18, 20, 23].

The structure of 0.7 mm thick sheets subjected to recrystallization annealing is characterized by equiaxed grains with a size gradient across the thickness (Figs. 1b, 2b), which is apparently associated with non-uniform heating during annealing. Despite the complete development of recrystallization and a decrease in maximum orientation density to 6.3, a pronounced texture is observed. The mechanisms of texture formation during recrystallization due to structural and textural heredity are described in [24–26]. The recrystallization texture is characterized by the presence of γ-fiber (Fig. 2b) with several maxima of individual components: strong {223}<142>, {332}<113> and weak {111}<110>. In ODF φ2 = 0 section, weak maxima {001}<210> and {001}<010> are noted, related to the θ-fiber, i.e. a set of orientations with the <001> axis parallel to ND. In addition, at approximately ¼ and ¾ of the thickness, individual grains with Goss orientation {110}<001> are observed and colored red in Fig. 1b. This orientation is characterized by extremely low intensity in ODF φ2 = 45° section.

Second cold rolling to a thickness of 0.26 mm results in an elongation of the grains in the rolling direction (Fig. 1c) and a slight increase in the orientation density to 7.65 (Fig. 2c). Despite the preservation of the γ-fiber, the maximum of orientation distribution intensity shifts towards {111}<110> orientation along with the formation of θ-fiber with a uniform density distribution (Fig. 2c). Therefore, three texture axes can be distinguished relative to CR coordinates: <110> ‖ RD, <111> ‖ ND and <001> ‖ ND.

Using the AZtec Crystal software, Young›s modulus was estimated from the EBSD data based on the additive contribution of each grain along four directions: RD, TD, 45° between them, and ND. Based on the data for the pure iron lattice from Aztec Crystal database the following flexibility matrix coefficients were used to calculate Young's modulus: C_{11} = 7.65, C_{12} = −2.79, and C_{44} = 8.56 1/TPa.

The Young's modulus color maps for 0.7 mm thick sheets after CR1 show a significant dispersion of values in ND, despite a uniform distribution in RD (Fig. 3b). The minimum values of elastic modulus are characteristic of the 45° direction (Fig. 3d), while the maximum values are observed in TD (Fig. 3c), which is confirmed by the modulus values depending on orientation distribution, represented in a form of pole figure (PF) (Fig. 6a).

Young's modulus is generally determined by interatomic forces and thus demonstrates significant anisotropy along crystallographic directions. The estimation of elastic moduli along the main crystallographic axes for GOES single crystals is provided in [27]: <110> — 214 GPa, <111> — 277 GPa, and <001> — 128 GPa. The analysis of elastic moduli values for individual orientations based on EBSD data demonstrates good agreement with the literature data. In particular, {001}<110> deformation cube orientation, which is colored green in (Fig. 3a) in RD according to the color key, corresponds to a value of 205 GPa (average modulus values). It is comparable to that in TD and has a minimum value (blue coloring) of 131 GPa in ND. The highest modulus values of 282 GPa are observed in ND for orientations close to {111}<112> and in RD for orientations close to {112}<111>. Each of these orientations is characterized by the <111> axis along the corresponding direction. It should be noted that Young's modulus for a given orientation exceeds its values for a single crystal in the highest modulus direction <111> by 5 GPa. The difference in elastic constants calculated using EBSD data and literature data is apparently due to the difference in flexibility matrix coefficients for iron provided in AZtec Crystal database and in [27]. The minimal integral Young's modulus for the 45° direction is due to the fact that for deformation cube orientation the <001> axis is predominantly parallel to the 45° direction.

Similar to the sheet after CR1, the Young's modulus structural maps of a 0.7 mm thick sheet after CR1 and RA are defined by uniform distribution in RD, while the

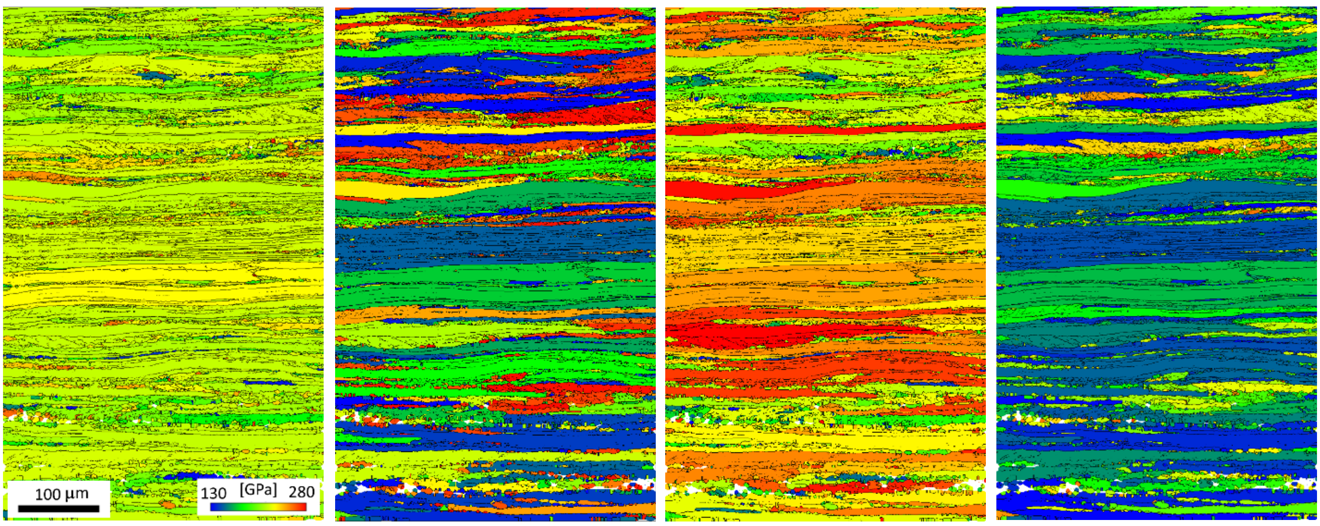

a b c d

Fig. 3. (Color online) Young's modulus structural maps for a 0.7 mm thick sheet after CR1 calculated from EBSD data for the following directions: RD (a), ND (b), TD (c), 45° between RD and TD (d).

greatest dispersion of values is typical for ND (Fig. 4). The minimum value of Young's modulus from the presented maps is characteristic of RD. It is difficult to determine the maximum value from structural maps due to a significant dispersion in ND. However, according to the PF data (Fig. 6b), the maximum value corresponds to TD. Moreover, during recrystallization, PF of Young's modulus rotates by 90° relative to the cold-formed state with the pattern preservation and a slight redistribution of pole densities, which is apparently accompanied by a decrease in elastic energy. It should be noted that there are series of grains with low Young's modulus values at ¼ and ¾, to a lesser extent at ½ of the sheet thickness in the RD, TD, and ND (Fig. 4a). According to texture analysis in RD, these areas (blue grains) correspond to Goss orientations {110} <001> (Fig. 4a), standard cube {100}<001>-orientations in TD, and a deformation cube — {001}<110> in ND (Fig. 4b,c). According to the data from [24,25,28], these orientations are nucleated during recrystallization at special boundaries formed between stable orientations during deformation.

For 0.27 mm thick sheets after CR2, uniform distribution is also observed in RD, while ND exhibits the greatest dispersion of values (Fig. 5a,b), which is also obvious from frequency histograms of the Young's modulus distribution (Fig. 7a,b). Even though ND (Fig. 5b) contains the greatest number of grains with the higher Young's modulus (colored red), maximum values in PF (Fig. 6c) are observed in TD. Despite the fact that the meridian pole density of modulus along 90° is uniform (including RD and ND), frequency distribution (Fig. 7b,c) for these directions as well as coloring in the structural maps are significantly heterogeneous. Frequency distribution in ND shows two maxima corresponding to the orientations close to {001}<110> and {111}<110>, with axes <001> and <111> parallel to ND, respectively. The <110> direction, common to these two orientations, yields one maximum of about 220 GPa in frequency distribution histograms in RD and TD (Fig. 7a,c).

Since the grain orientation has the greatest influence on the Young's modulus values, the obtained texture data for the sheets in different structural states were used to estimate the

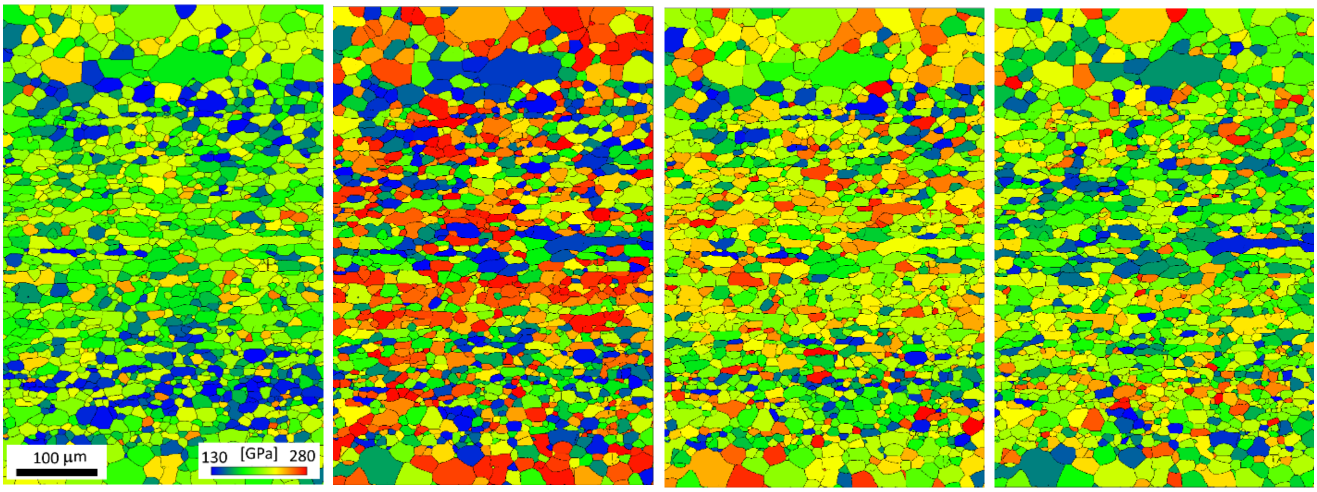

a b c d

Fig. 4. (Color online) Young's modulus structural maps for a 0.7 mm thick sheet after CR1+DRA calculated from EBSD data for the following directions: RD (a), ND (b), TD (c), 45° between RD and TD (d).

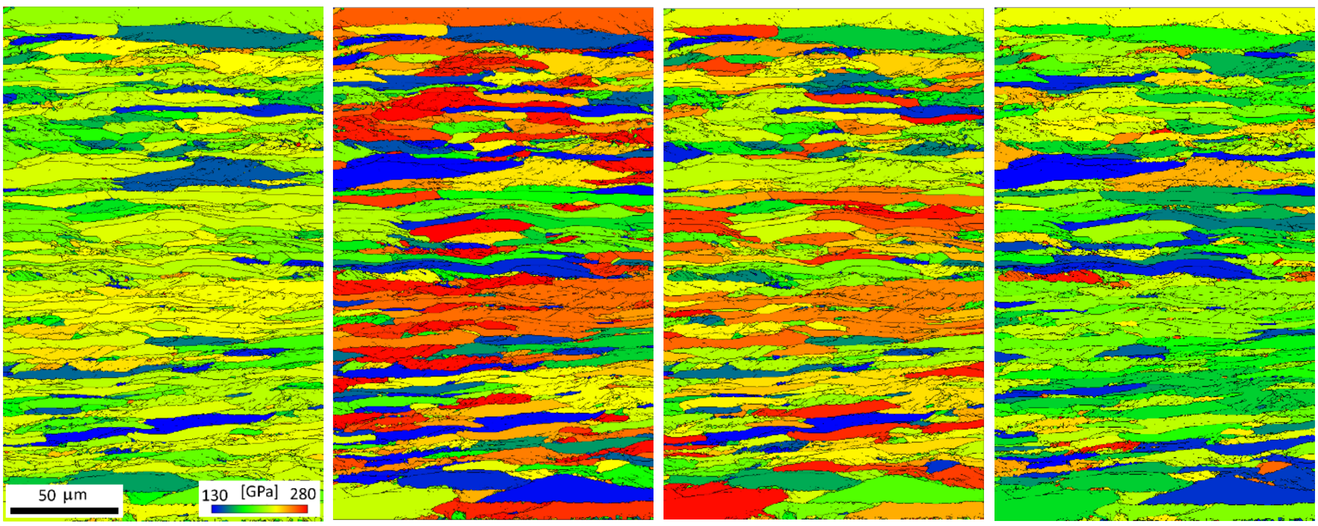

a b c d

Fig. 5. (Color online) Young's modulus structural maps for a 0.27 mm thick sheet after CR2, calculated based on EBSD data in: RD (a), ND (b), TD (c), 45° between RD and TD (d).

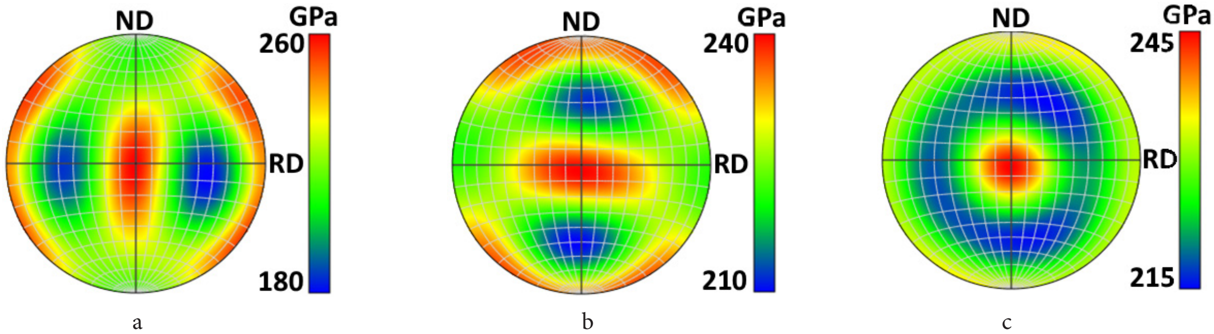

Fig. 6. (Color online) Young's modulus distribution in a form of PF for in GOES sheets at different processing stages: 0.7 mm sheet after CR1 (a), 0.7 mm sheet after CR1+DRA (b), 0.27 mm sheet after CR2 (c).

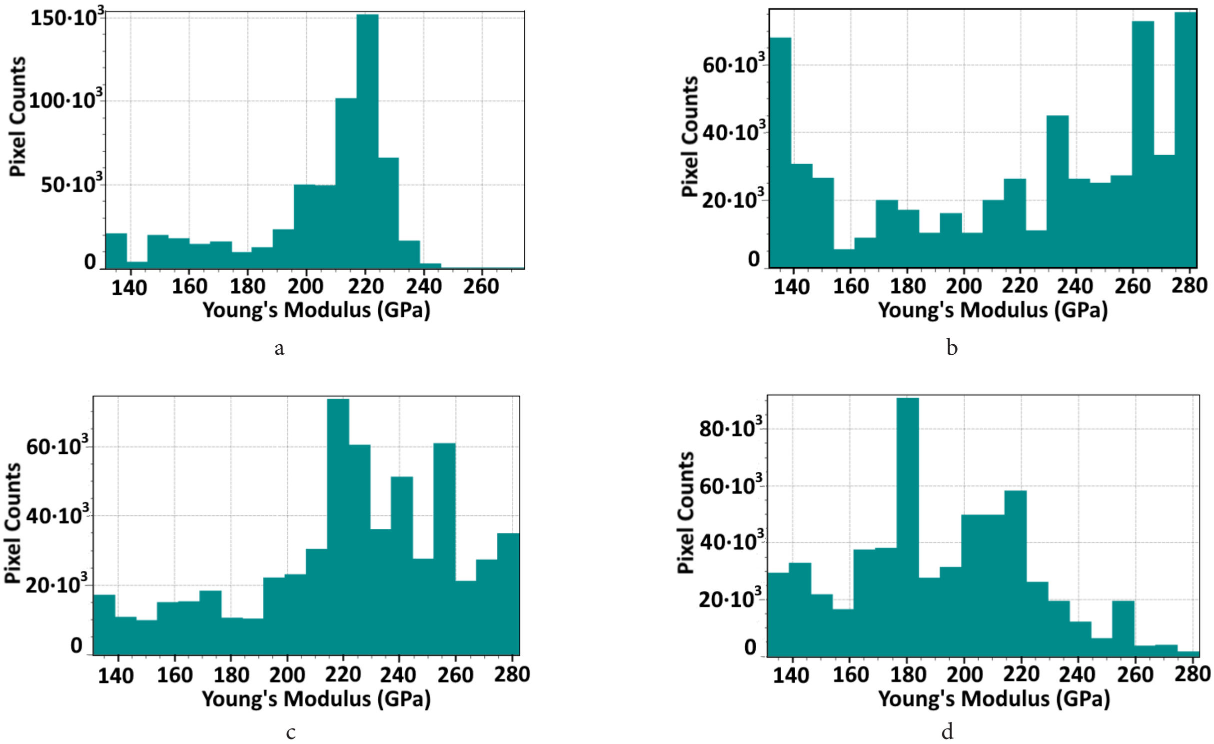

Fig. 7. Young's modulus frequency distribution calculated from EBSD data for a GOES sheet with a 0.27 mm thickness after CR2 in: RD (a); ND (b); TD (c); 45° (d).

proportion of orientations with <100>, <110>, and <111> axes deviating by less than 20° from the RD and TD, and 45° between RD and TD (Fig. 8). The CR1 sheet exhibits a higher proportion of low-modulus orientation <100> in the 45° direction, <110> in the RD, and <111> in the TD compared to the other two structural states. This is due to the highest texture sharpness at this stage and specifically due to the deformation cube texture typical for CR1. The recrystallized state is defined by a sufficiently uniform <110>-orientations distribution, which is apparently due to the fact that <110> is the main rotation axis of recrystallized grains according to [23]. Sheets after DRA and after DRA and CR2 are characterized by grains with a predominant low-modulus <100> direction along RD, and high-modulus <111>-direction in TD.

Using standard tensile testing or measuring the speed of sound for the estimation of Young's modulus of thin sheets is methodologically challenging due to requirements for the shape and size of specimens. Dynamic mechanical analysis (DMA) can be an appropriate method for thin plates as specimens. It is based on the excitation of sinusoidal mechanical vibrations and recording the stress-deflection relation during three-point bending. This method allows one to determine the so-called storage modulus E', which indicates the amount of retained applied load in the material as elastic potential energy [29].

The analysis of storage modulus anisotropy in comparison with averaged Young's modulus calculated from EBSD data for 0.7 mm thick sheets demonstrates comparable values. Specifically, both elastic characteristics of the sheet after CR1 are maximal in the TD and minimal in the 45° direction. For the sheet after CR1 and DRA the minimum value is observed in RD and maximum in TD, which is consistent with the estimated proportion of <100>, <110>, and <111> orientations (Fig. 9).

While the values are generally comparable, greater anisotropy and lower modulus values along RD and TD are observed for the sheet after CR2 according to DMA data compared to EBSD data. This difference for the thinner sheet (0.27 mm) can be explained by the greater contribution

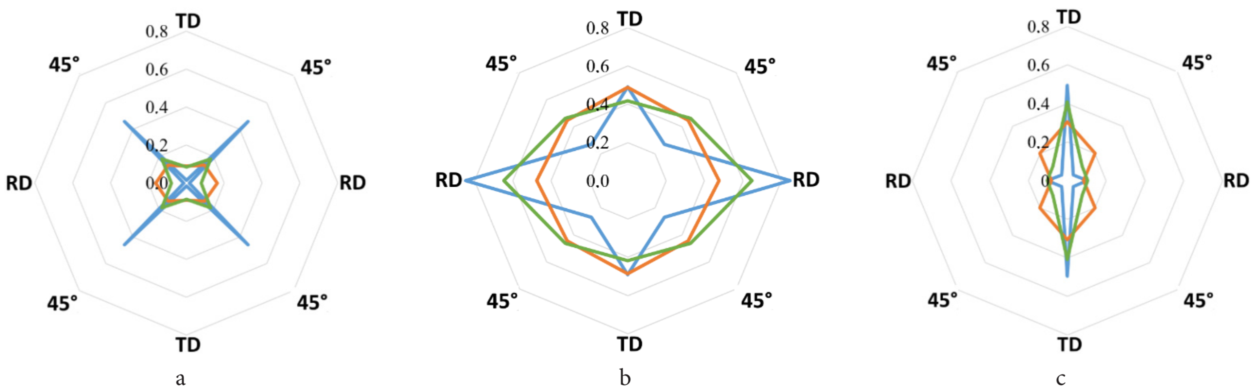

Fig. 8. (Color online) The frequency distribution of the grains with orientations <001> (a), <110> (b), <111> (c) estimated along cold rolling axes for GOES sheets at different processing stages: 0.7 mm thick after CR1 (blue), 0.7 mm thick after CR1+DRA (orange), 0.27 mm thick after CR2 (green).

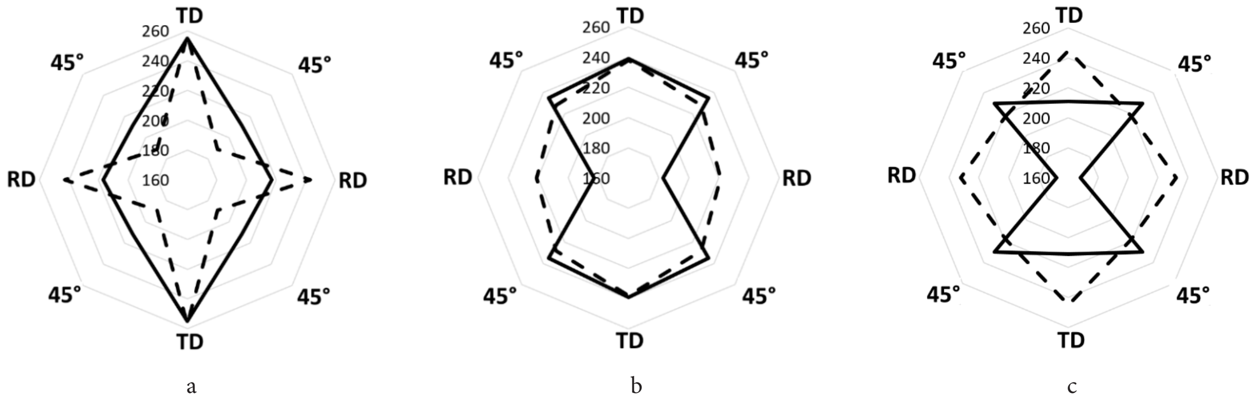

Fig. 9. Young's modulus orientation dependence obtained from DMA (solid line) and EBSD (dashed line) data for GOES sheets: 0.7 mm thick after CR1 (a), 0.7 mm thick after CR1+DRA (b), 0.27 mm thick after CR2 (c).

of near surface layers to the overall elastic modulus. This parameter gains an even greater influence considering the three-point bending pattern during DMA and uneven stress distribution across the sheet thickness. During bending, maximum stresses occur in the surface layers, which experience a greater elastic response.

4. Conclusions

The structure and texture evolution of cold-rolled GOES sheets was studied at various stages of cold rolling and heat treatment:

1. The combination of cold rolling and intermediate recrystallization annealing leads to the formation of a texture with specific axes <110>‖RD (α-fiber), <111>‖ND (γ-fiber) and <001>‖ND (θ-fiber). In addition, for the 0.7 mm thickness sheets subjected to recrystallization annealing, a structure gradient across the thickness is noted, which is characterized by larger near-surface grains and the formation of individual grains with a Goss texture {110}<001> at ¼ and ¾ of the thickness.

2. The elastic moduli anisotropy of GOES sheets after various thermal and deformation treatments was estimated along with the comparative analysis of elastic moduli measured by DMA and EBSD. A correlation between values obtained by two different methods was established. However, a larger divergence in the elastic moduli values was observed for the 0.27 mm thick sheet due to the stress state features observed during DMA measurements, which results from the greater elastic deformation of near-surface layers typical for three-point bending.

3. A relationship was established between the crystallographic texture of GOES sheets and the formation of Young's modulus anisotropy at various stages of heat treatment and deformation processing. During recrystallization, the pole density pattern of Young›s modulus values rotates by 90°. For all investigated samples, the uniform distribution of Young's modulus was found in RD, with the elastic modulus maximum values in TD. The greatest dispersion of values corresponds to ND, which is in good agreement with the texture analysis based on the proportion of common orientations characterized by preferred <100>, <110> and <111> axes.

References

1. A.A. Redikultsev, M.L. Lobanov, M.A. Zorina, D.D. Satskii, Mechanism of structural-textural heredity in grain oriented electrical steel. 1. Secondary recrystallization, Metal Science and Heat Treatment, 3 (2025) 3–9. (in Russian)
2. A.A. Redikultsev, M.L. Lobanov, M.A. Zorina, D.D. Satskii, Mechanism of structural-textural heredity in grain oriented electrical steel. 2. Evolution of the main crystallographic orientations, Metal Science and Heat Treatment, 3 (2025) 10–17. (in Russian)

3. K. Fujisaki, Fundamental Concept of Magnetic Material for Electrical Engineer, in: Handbook of Magnetic Material for Motor Drive Systems, Springer Nature Singapore, Singapore, 2025, pp. 1–19.
4. T. Kumano, T. Haratani, Y. Ushigami, The Relationship between Primary and Secondary Recrystallization Texture of Grain Oriented Silicon Steel, ISIJ International 42 (2002) 440–449.
5. Y. Hayakawa, Mechanism of secondary recrystallization of Goss grains in grain-oriented electrical steel, Sci. Technol. Adv. Mater. 18 (2017) 480–497.
6. C. Yilmaz, M. Poul, L. Lahn, D. Raabe, S. Zaefferer, Dislocation-assisted particle dissolution: A new hypothesis for abnormal growth of Goss grains in grain-oriented electrical steels, Acta Mater. 258 (2023) 119170.
7. F. Lifeng, Z. Tiannan, G. Jun, X. Lijun, Y. Erbin, L. Hongbin, C. Liansheng, Coordinate regulation mechanism of primary recrystallization texture and microstructure of grain-oriented silicon steel, Metallurgical Research & Technology 121 (2024) 510.
8. M.L. Lobanov, A.A. Redikultsev, M.A. Zorina, Metalphysics of materials for electromechanical engineering, Ekaterinburg Ural University Publisher House, 144 p. (in Russian)
9. S. Chu, B. Zhou, B. Mao, State of the art and prospects on the metallurgical design and manufacturing process of grain-oriented electric steels, J. Magn. Magn. Mater. 614 (2025) 172739.
10. Y.N. Loginov, S.I. Stepanov, M.P. Puzanov, A.G. Nezhdanov, Influence of Cold Rolling Temperature Rise on the Young's Modulus of Commercial Fe-3%Si Steel, KnE Engineering 1 (2019) 113–120.
11. Y.N. Loginov, M.P. Puzanov, Influence of properties anisotropy on stress-deformed state at rolling of stripes from electrical STEEL, Chernye Metally 1042 (2018) 22–27. (in Russian)
12. F. Gao, Y. Chen, Q. Zhu, Y. Nan, S. Tang, Z. Cai, F. Zhang, W. Xue, X. Cai, F. Yu, Z. Liu, Formation of recrystallization texture and its effect on deep drawability for high-purified ferritic stainless steel by two step cold rolling, Mater. Des. 226 (2023) 111679.
13. F. Gao, Q. Zhu, W. Xue, Y. Chen, F. Zhang, Y. Nan, S. Tang, J. Zhang, D. Tie, X. Cai, F. Yu, Z. Liu, Correlation between formability, ridging and recrystallization texture development in ferritic stainless steel fabricated by introducing intermediate annealing during cold rolling, Mater. Charact. 205 (2023) 113296.
14. C.O. Stasac, A.D. Tomșe, M.N. Arion, L. Bandici, F.I. Hathazi, Effect of Heat-Treatment Process on Magnetic Characteristics of Grain-Oriented Electrical Steel, Processes 12 (2024) 2045.
15. G. Nithyanandh, S.K. Yogeshwaran, S. Santosh, Preparation, characterization and dynamic mechanical analysis of CuZnAl shape memory alloys, Mater. Today Proc. (2023) 2476–2479.
16. A.K. Mohamed, M.Y. Zadorozhnyy, Y. Mansouri, I.S. Golovin, Magnetostriction and damping of forced vibrations in Fe-Cr-Mo-Al alloy, Mater. Lett. 314 (2022) 131863.
17. M. Seehaus, S.H. Lee, T. Stollenwerk, J.M. Wheeler, S. Korte-Kerzel, Estimation of directional single crystal elastic properties from nano-indentation by correlation with EBSD and first-principle calculations, Mater. Des. 234 (2023) 112296.
18. M. Hölscher, D. Raabe, K. Luecke, Rolling and recrystallization textures of bcc steels, Steel Research 62 (1991) 567–575.
19. F.J. Humphreys, M. Hatherly, Recrystallization and related annealing phenomena second edition, 2nd ed., Elsevier Ltd., Oxford, 2004.
20. V. Tandon, K.S. Park, R. Khatirkar, A. Gupta, S.H. Choi, Evolution of Microstructure and Crystallographic Texture in Deformed and Annealed BCC Metals and Alloys: A Review, Metals (Basel) 14 (2024) 149.
21. Y. Fu, L. Fan, Microstructure and Texture Evolution of High Permeability Grain-Oriented Silicon Steel, Metals (Basel) 15 (2025) 268.
22. S. Satyam, David P. Field, Advances in Texture, Microtexture, and Allied Techniques, 1st ed., Materials Horizons: From Nature to Nanomaterials, 2025.
23. M.L. Lobanov, S.V. Danilov, V.I. Pastukhov, S.A. Averin, Y.Y. Khrunyk, A.A. Popov, The crystallographic relationship of molybdenum textures after hot rolling and recrystallization, Mater. Des. 109 (2016) 251–255.
24. A.A. Redikul'tsev, M.A. Zorina, V.I. Pastukhov, M.L. Lobanov, The role of special boundaries in structural and phase transformations in metals and alloys. 1. Deformation and recrystallization, Metal Science and Heat Treatment 9 (2025) 6–11. (in Russian)
25. A.A. Redikul'tsev, M.A. Zorina, V.I. Pastukhov, M.L. Lobanov, The role of special boundaries in structural and phase transformations in metals and alloys. 2. Phase transformations, Metal Science and Heat Treatment 9 (2025) 12–18. (in Russian)
26. K. Traka, E.S. Hernández, T. Nguyen-Minh, K. Sedighiani, J. Sietsma, L.A.I. Kestens, Prediction of different recrystallisation textures under a single unified physics-based model description, Comput. Mater. Sci. 246 (2025) 113425.
27. S. Takaki, T. Masumura, T. Tsuchiyama, Young's Modulus of Single Crystalline Iron and Elastic Stiffness, Tetsu-to-Hagane 9 (2020) 679–682.
28. R. Matsubara, Y. Ushigami, Effects of Coincidence Site Lattice (CSL) Grain Boundaries on Secondary Recrystallization in Heavily Cold-rolled Grain-oriented Electrical Steel, ISIJ International 65 (2025) 2242–2251.
29. S. Ebnesajjad, P.R. Khaladkar, Fluoropolymers Applications in the Chemical Processing Industries, Delaware, William Andrew Publishing, 2005, 452 p.